Laser-ultrasonic attenuation and absorption measurements in metals

Perton, M.; Lévesque, D.; Moreau, A.; Lamouche, G.; Monchalin, J.-P.

Publisher's version / Version de l'éditeur:
https://doi.org/10.1063/1.4716235
Review of Progress in Quantitative Nondestructive Evaluation: Burlington, Vermont, USA, 17-22 July 2011, AIP Conference Proceedings; Volume 1430, pp. 235-242, 2011-07-17

LASER-ULTRASONIC ATTENUATION AND ABSORPTION MEASUREMENTS IN METALS

M. Perton, D. Lévesque, A. Moreau, G. Lamouche, and J.-P. Monchalin

Industrial Materials Institute, National Research Council of Canada, 75 de Mortagne, Boucherville, Québec, Canada, J4B 6Y4

ABSTRACT. The attenuation of an acoustic wavefront in metals comes from scattering caused by grain anisotropy and random grain orientation and from absorption caused by mechanisms such as dislocation and magnetic domain motion. In this paper laser ultrasonics, with its non-contact and broadband characteristics, is used for measuring and separating these two attenuation contributions as a function of frequency. Results obtained from the well-known pulse-echo method and reverberation technique are presented first. Then, a more recent approach using a time-frequency analysis with zero-group velocity (ZGV) resonances is considered. It is shown that the attenuation with scattering and absorption components is obtained by fitting the temporal decay of the resonances of the coherent field, and that only the absorption component is obtained from the temporal decay of the diffuse field between resonances.

Keywords: Laser Ultrasonics, Ultrasonic Absorption, Scattering, Diffusion Regime, Zero Group Velocity
PACS: 78.40.Kc, 43.35.Cg, 81.70.Cv

INTRODUCTION

The attenuation of a coherent wavefront in polycrystalline metals is due to diffraction, absorption, and scattering. Diffraction can be controlled by choosing well-suited source and detection dimensions, or minimized if the plane-wave assumption or near-field is achievable. Absorption phenomena are diverse and include dislocation motion, magnetic domain motion. Scattering depends upon frequency, wave polarization, and the size, anisotropy and orientation distribution of grains. With the diffraction effect removed, the attenuation contributions are described approximately by frequency power laws as:

$$\begin{aligned} \alpha_{att}(\omega) &= \alpha_{abs}(\omega) + \alpha_{sca}(\omega) \\ &= C_{abs}\omega^{p} + C_{sca}\omega^{q} \end{aligned}, \tag{1}$$

where $\omega = 2\pi f$, f is frequency, the exponent p is between 0.1 and 2 [1] and the exponent q is typically between 2.5 and 4 [2]. Also, it is found that the ratio between coefficients C_{abs} and C_{sca} is temperature dependent [3]. Because of these components, the displacement field in a metal can be seen as the combination of a coherent field and a scattered field:

$$u(x,t) = u_{coh}(x,t)e^{-(\alpha_{abs}+\alpha_{sca})t} + u_{sca}(x,t)e^{-(\alpha_{abs})t} \tag{2}$$

The coherent field is attenuated by absorption and scattering. The scattered field arises from the scattered coherent field and is only attenuated by absorption. After enough scattering events, the scattered field becomes diffuse, and thus only affected by absorption.

The separate measurements of the scattering and absorption components are very useful for materials characterization. Several techniques have this purpose and some of them are reviewed in this paper. It is noticed first that the scattered field displacement is measured only if the size of the detection area is smaller than the spatial coherence length in the ultrasonic frequency range considered. Accordingly, the coherent field is often measured with large area detection to average out the diffuse field, while the diffuse field is usually measured with small probes. Another way to separate the two contributions is by choosing an appropriate time window in the signal: the coherent field is more important at the early stage and the scattered field is predominant at longer time. The pulse-echo technique [4, 5] is used at early times and is described first. Then, the reverberation technique [6-7] used at longer times will be discussed. The purpose of this paper is to clarify what happens at intermediate times, when coherent and scattered fields are detected simultaneously, in particular with diffusion of the scattered field in an unbounded plate [8, 9] or with the presence of zero group velocity (ZGV) resonance modes [10]. The laser-ultrasonic technique with its non-contact and broadband characteristics is used for measuring the two contributions as a function of the frequency. All the experiments are performed in carbon-manganese 1008 steel. This allows comparing the results from the different techniques.

CLASSICAL APPROACHES

Pulse-Echo Technique

The pulse-echo technique [4, 5] is based on the analysis of propagation of a broadband pulse generated on a plate with parallel faces. After being reflected by the back surface, the reflected pulse shows the effect of attenuation over a distance $2e$, where e is the sample thickness. The echoes resulting from the back and forth propagation of the pulse are windowed in time and their spectra should show a good signal-to-noise ratio (SNR). The ratio of the spectra of two consecutives echoes leads to the attenuation according to the relation:

$$\alpha_{att}(\omega) = \frac{20\log_{10}(A/B) - D}{2e}, \tag{3}$$

where A and B are the amplitude spectra of the first and second echoes, respectively. D is a correction factor for diffraction and is negligible when propagation is in the near-field. Using a large detection spot also allows removing the scattered field and, consequently, improves the SNR. Another way to overcome the diffraction correction is by using a single echo from the test sample and a reference echo from a sample of comparable thickness with negligible or known attenuation in the same measurement conditions [1].

In the experiment, the acoustic generation was realized by a Q-switched Nd:YAG laser operating at a wavelength of 1064 nm, with a pulse duration of 8 ns, and a pulse energy of about 1.5 J in the ablation regime. The spot diameter was about 1 cm. The measurement was made in transmission using a 100 mJ long-pulse (~1 ms) Nd:YAG laser operating at a wavelength of 1064 nm. The laser spot diameter was about 4 mm. The reflected light was then collected and demodulated with a 0.5 m confocal Fabry-Perot interferometer operating in the reflection configuration. Finally, the signal was normalized by the temporal profile of the detection laser pulse.

Reverberation Technique

Several methods have been proposed for only measuring the absorption in scattering media among which there is the reverberation technique [6]. In this technique a broadband acoustic pulse is generated on a small and physically isolated sample. Rapidly, the acoustic field fills the sample volume and loses its coherence because of grain scattering and geometrical irregularities. Soon after, the scattered field tends to be diffuse, the scattering has no more incidence over the local mean energy density and the temporal decay at a given frequency is only function of the absorption. The use of laser ultrasonics was introduced later to allow a non-contact and more broadband measurement [7].

In the present experiment, a small coupon was cut from a 2 mm thick 1008 steel plate in the shape of an irregular polygon (more than 8 edges) with an approximate surface of 4 cm^2. In order to have a good SNR over a large frequency bandwidth, two experimental setups were used. The first one is well suited for frequencies below 15 MHz. It is the same setup as in the pulse-echo technique, but the generation pulse energy is 1 J over a round spot of 4 mm diameter, and the detection spot diameter is 20 µm with an energy adjusted to be just below the ablation threshold. The second setup is better suited for frequencies between 15 and 40 MHz. The acoustic generation was realized by a Nd:YAG operating at a wavelength of 355 nm, with a pulse duration of 35 ps, a pulse energy of 7 mJ, and focused onto a round spot of 2 mm diameter. The generation is in the thermoelastic regime and temporal averaging of 400 signals was required. The detection was the same as for the other setup. Also an electronic high-pass filter (> 10 MHz) was added to eliminate the large-amplitude low-frequency components and increase the dynamic resolution at high frequencies when digitizing the signal. For both setup, several signals were recorded at different locations and their time-frequency representations (TFR) are averaged using short-time Fourier transforms. This allows averaging the scattering contributions or the geometrical irregularities. Figure 1 shows the signal obtained, the TFR, and the amplitude decay as function of time at one specific frequency (5 MHz) and fitted by the equation:

$$\left|u_{TFR}(\omega,t)\right| = c_1 e^{-\alpha_{abs} t} + c_2 , \qquad (4)$$

where c_1, c_2, and α_{abs} are the fitted parameters.

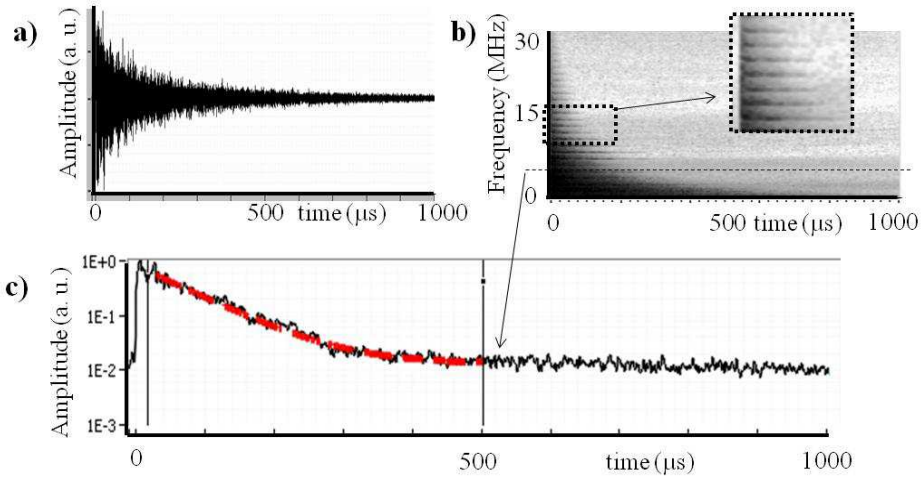

FIGURE 1. a) Signal obtained from the reverberation experiment, b) corresponding TFR (black is high amplitude, white is low amplitude), and c) amplitude decay at a given frequency from b) (black noisy curve) and fitted with Eq. 4 (dashed curve).

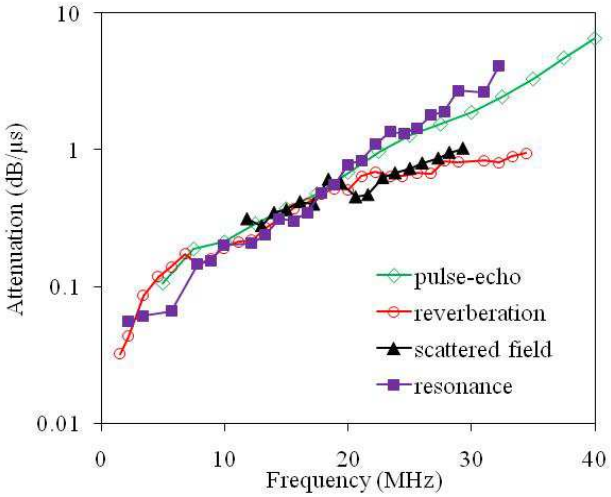

FIGURE 2. Longitudinal attenuation and absorption measured as function of frequency using the different techniques for a 1008 steel sample.

Measurement Results and Discussion

The results of the two techniques are reported in Fig. 2. The pulse-echo technique allows measuring the total attenuation comprising the scattering and absorption components while the reverberation technique provides only the absorption component. Since longitudinal echoes were used in the pulse-echo technique, the absorption of the longitudinal mode should be considered for comparison with the reverberation technique. Indeed, it can be shown [11, 12] that the resonances observed in the diffuse field, such as in Fig. 1b at frequencies higher than 8 MHz (see magnification), can be associated to the longitudinal mode. The resonances emerge from the background only above 8 MHz because the mean free path becomes smaller than the lateral dimension of the coupon. In Fig. 2, the points of the absorption curve for frequencies higher than 8 MHz were obtained by fitting the amplitude decay on each resonance frequency, the 2 mm coupon thickness providing a sufficient number of longitudinal resonances. For frequencies lower than 8 MHz, no clear resonance peak is identified so that amplitude decay results are not representative of purely longitudinal absorption. Also at low frequencies, the diffuse regime takes more time to be reached, and the amplitude decay might have been estimated before actually reaching the diffusion regime. Considering the logarithmic scale for the attenuation, it can be deduced that the absorption component dominates at frequencies below 20 MHz. The scattering component is predominant at higher frequencies.

DIFFUSION TECHNIQUES

Diffusion of the Scattered Field in a Plate

The diffusion technique was proposed first by Guo et al. [8] and a laser-ultrasonic version has also been reported [9]. This technique is quite similar to the reverberation technique, but uses an unbounded plate. Consequently, the scattered field can escape in the lateral dimensions and it is not possible to link directly the temporal decay of the signal with absorption. However, it has been shown that the absorption coefficient can be deduced from a deeper analysis of the signal measured. Soon after the generation of a localized acoustic pulse, a scattered field results from the coherent field, becomes diffuse and is detected at a distance, r, from the generation area. The energy, E, associated to the diffuse field is described by a diffusion equation:

$$\frac{\partial E}{\partial t} = D_{dif}(\omega)\nabla^2 E - 2\alpha_{abs}(\omega)E, \tag{5}$$

where D_{dif} is the diffusion coefficient, and has the solution:

$$E(\boldsymbol{r},\omega,t) \propto \exp\left(-\frac{r^2}{4D_{dif}(t-t_0)} - 2\alpha_{abs}t\right) \Big/ \sqrt{2D_{dif}(t-t_0)^m}, \tag{6}$$

where t_0 is the initial time of the diffusion regime and m is the spatial dimensions of the energy diffusion, which is not necessarily the dimension of the problem. In a 3D plate for example, with a thickness shorter than the mean free path, the diffuse field fills rapidly the thickness and diffusion occurs only along the plate (with a point source, m=2; with a line source, m=1). The solution (6) assumes that the diffuse field is a point at t=t_0. In the case of laser generation, the radial profile of the spot can be considered Gaussian. It is then assumed that the initial spatial distribution of the diffuse field, which results from scattering of the coherent acoustic pulse, will also be Gaussian, but with a larger radius characterized by σ_{dif}. When convolved by this spatial distribution, the solution to equation (5) is:

$$E(\boldsymbol{r},\omega,t) \propto \frac{e^{-\frac{r^2}{4D_{dif}(t-t_0)+2\sigma_{dif}{}^2} - 2\alpha_{abs}t}}{\sqrt{\left(2D_{dif}(t-t_0)+\sigma_{dif}{}^2\right)(t-t_0)^{(m-1)}}}. \tag{7}$$

The coefficients σ_{dif} and t_0 are difficult to determine but become insignificant at large times. By fitting the experimental results for several distances, r, with this expression, the absorption and the diffusion coefficient are obtained. The diffusion coefficient has been found to correlate with grain size [9].

Diffusion-like Behavior of the Coherent Field at the Resonances

The diffusion technique is valid only if the scattered field is more important than the coherent field, and assumes that the coherent field is far from the measurement point or is totally scattered. In a plate, however, it has been reported recently that some acoustic modes of the coherent field do not propagate in the sense that their group velocity is zero [10]. These zero group velocity (ZGV) modes correspond to the points where $\partial\omega/\partial k_r = 0$ on the (k_r,ω) dispersion curves (where k_r is the horizontal component of the wave vector $\boldsymbol{k}$). The vicinity of those ZGV points has a very low group velocity and the energy contained in a narrow frequency interval around the ZGV mode may be considered diffusive. It is thus useful to describe the time decay of such modes.

Prada et al [10] have described the temporal decay of ZGV modes for $k_r \neq 0$ by:

$$\left|u(\boldsymbol{r},t,\omega^{ZGV})\right| \propto J_0\left(k_r^{ZGV} r\right) e^{-\alpha t}/\sqrt{t}. \tag{8}$$

Here, the temporal decay of the ZGV modes with $k_r = 0$, corresponding to through-thickness longitudinal mode resonances, is considered. The derivation is made supposing an isotropic medium and a line source (*i.e.* a problem with 2 dimensions) and then generalized to a point source (*i.e.* a problem with 3 dimensions). In what follows, r stands for the distance along the plate surface (Cartesian or radial coordinate according to the dimensions) and z for the distance along the thickness. The coherent field is written as a plane-wave decomposition:

$$u_{coh}(r,z,t) = \iint A(\boldsymbol{k}) e^{i(\omega t - k_r r - k_z z)} \mathrm{d}k_r \mathrm{d}\omega, \tag{9}$$

where we isolate:

$$\tilde{u}\left(k_r,k_z,t,r,z\right)=A\left(\boldsymbol{k}\right)e^{i\left(\omega t-k_r r-k_z z\right)}. \tag{10}$$

The resonance frequency of the n^{th} harmonics is expressed as a function of the complex phase velocity c_L^* which takes into account the attenuation:

$$\omega_n\left(k_r=0\right)=\frac{n\pi c_L^*}{e}=\omega_n^R+i\alpha_{att}, \tag{11}$$

where ω_n^R is the real part of ω_n. Then, the angular frequency around the resonance point is expressed in a Taylor series expansion:

$$\omega_n\left(k_r\right)=\omega_n\left(0\right)+D_{disp}{k_r}^2. \tag{12}$$

An analytical expression of D_{disp} is obtained for isotropic material by introducing Eq. (12) in the Rayleigh-Lamb equation and by using the limit when k_x tends toward 0:

$$D_{disp}=\left|\frac{{c_L^*}^2}{2\omega_n}+\frac{8{c_T^*}^3}{e{\omega_n}^2\tan\left(\omega_n e/2c_T^*+a\right)}\right|,\left(a=\begin{cases}0 & :\text{if n odd}\\ \pi/2 & :\text{if n even}\end{cases}\right). \tag{13}$$

By taking into account Eqs. (11), (12) in the time derivative and the Laplacian (along the horizontal direction only) of $\tilde{u}$, it is found that the displacement around the resonance frequency satisfies a diffusion-like equation with complex numbers:

$$\frac{\partial\tilde{u}}{\partial t}=\left(i\omega_n^R-\alpha_{att}\right)\tilde{u}-iD_{disp}\Delta\tilde{u}, \tag{14}$$

The solution to this equation, convolved by the spatial laser distribution (source and detection) σ, and generalized to dimension m (the horizontal dimensions according to the Laplacian) is equal to:

$$\left|\tilde{u}\right|\propto\left|\exp\left(-\frac{r^2}{2\sigma^2-4iD_{disp}t}-\alpha_{att}t\right)\middle/\sqrt{\left(\sigma^2-2iD_{disp}t\right)t^{(m-1)}}\right|. \tag{15}$$

This solution is independent of k_r, so the integration over k_r around a resonance frequency in Eq. (9) is straightforward. In order to validate this result, a theoretical simulation was performed of the displacement generated by a normal and suddenly applied force (representative of the ablation regime) on a homogeneous isotropic plate including viscoelasticity, but without scattering.

Figure 3 shows the simulated signal and the corresponding TFR. The longitudinal resonances ($k_r=0$) appear as equi-spaced horizontal lines in Fig. 3b. The resonances associated to the ZGV modes with $k_r\neq0$ correspond to the others horizontal lines. A transient displacement associated to the propagating waves (all k_r) can also be observed before 5 µs at all frequencies. The influences of the distance r, the source-detection size σ, and the diffusion dimension m (m=2 for a point source and m=1 for a line source) were tested by fitting the simulated signal filtered around each harmonic with Eq. (15). The influence of D_{disp}, which is function of ω_n, was also tested for all harmonics. Figure 3c shows an example of the good agreement between the filtered signal and the fitted curve after the transient waves have disappeared (after 5 µs).

The numerical simulation was performed using a Kelvin-Voigt absorption model with the complex stiffness tensor $C^* = C(1+i\eta\omega)$, where the absorption, η, is a scalar. Therefore, this model assumes identical longitudinal and shear absorption values. It is shown as the red curve in Fig. 3d. The absorption values fitted on the resonance frequencies of the longitudinal mode using Eq. (15) (points) and of the ZGV modes with $k_r\neq0$ using Eq. (8) (squares) are found in good agreement with the absorption model.

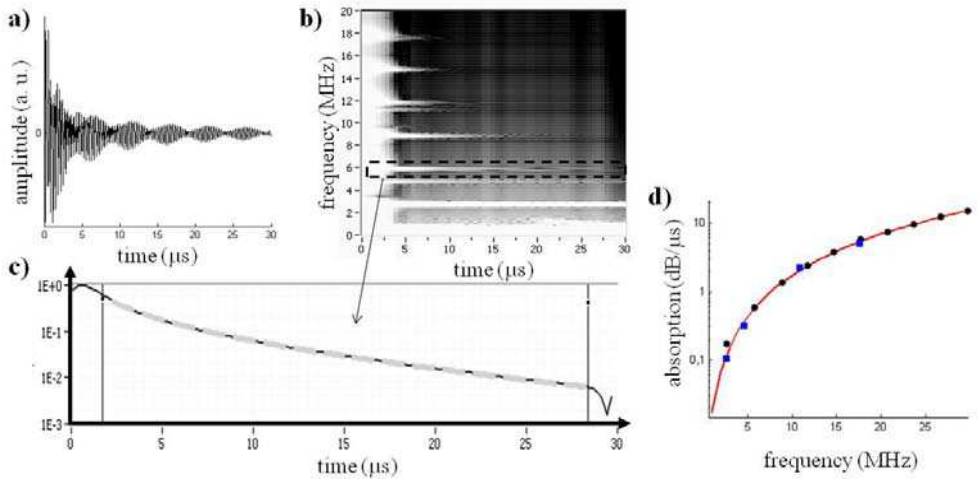

FIGURE 3. a) Simulated signal, b) corresponding TFR, c) amplitude filtered around the resonance indicated in "b)" (black curve) and fitted with Eq. 15 (gray dashed curve), and d) theoretical absorption included in the simulations (line), absorption values fitted on the longitudinal resonance frequencies (circles) and on ZGV resonance modes (squares).

Measurement Results and Discussion

Figure 4 presents the TFR of measured signals using an experimental setup quite similar to the one described with the pulse-echo technique. In the first measurement shown in Fig. 4a, a large detection spot of 2 mm was used to integrate and remove the scattered field. In the second measurement in Fig. 4b, a small detection spot of 20 µm was used to sense the scattered field.

The total attenuation was estimated by fitting the time decay at various resonant frequencies of the Fig. 4a with Eqs. (8) and (15). In Fig. 4b, the displacement appearing between the resonances is only due to the scattered field, and it temporal decay is used for determining absorption when fitting it with Eq. (7). On the resonances, the displacement is due to the superposition of the coherent and scattered fields. The temporal decays of that resonances are nevertheless similar to those of Fig. 4a, showing that the energy of the coherent field is much greater than that of the diffuse field. Attenuation results of both experiments are presented in Fig. 2 and are consistent with the results obtained from the pulse-echo and reverberation techniques. The absorption was not obtained at low frequencies because the mean free path was larger than the plate size and reflections of the coherent field on the edges disturb the diffuse field.

As a remark, the measurement precision increases by fitting only at late times where the influence of the source size decreases. Therefore asymptotically, the displacement of the diffuse field decays as $e^{-\alpha_{abs}t}/t^{m/4}$, the displacement of the ZGV mode with $k_r \neq 0$ (resp. $k_r = 0$) decays as $e^{-(\alpha_{abs}+\alpha_{sca})t}/t^{1/2}$ (resp. $e^{-(\alpha_{abs}+\alpha_{sca})t}/t^{m/2}$). One notices that, in a plate, the dimension for the diffusion of the ZGV modes with $k_r \neq 0$ always corresponds to m=1, whatever the source (line source or point source). The reason that m = 1, even with a point source, is that the diffusion-like behavior of the wave vector takes place only in one dimension, the radial direction and not along the angular direction because of the axi-symmetry of the problem. Also with a point source, the diffusion of ZGV modes has the same asymptotic time dependence as the diffusion of the scattered field, i.e. $t^{-1/2}$.

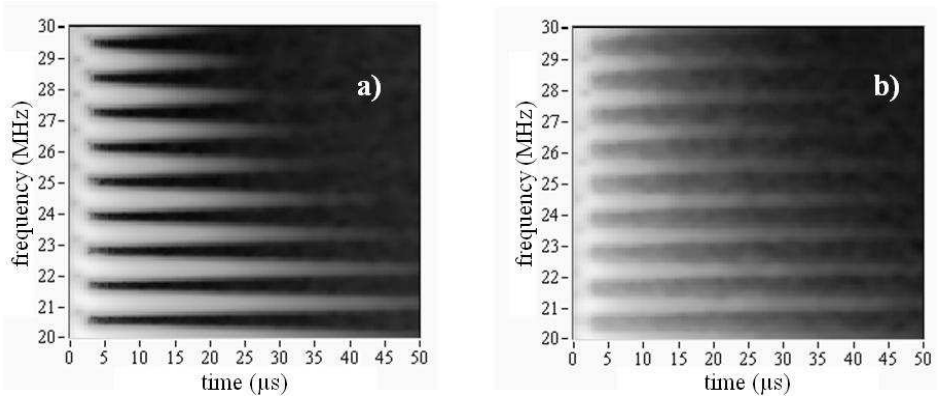

FIGURE 4. Measurement results with a) a 2 mm detection spot and b) a 20 μm detection spot in an unbounded plate.

CONCLUSIONS

The scattering and absorption components of ultrasonic attenuation in 1008 steel were characterized as a function of frequency using laser-ultrasonics. The pulse-echo, reverberation, and diffusion techniques were reviewed, employed and compared. A new technique using the diffusion-like behavior (caused by velocity dispersion) of ZGV modes in a plate was presented and used to measure the total attenuation. It also provided new insights into the interpretation of the diffusion technique at the longitudinal resonances. Also, different expressions for the temporal decay of the measured displacement with this technique are derived.

ACKNOWLEDGEMENTS

The authors would like to thank Martin Lord for his assistance in instrumentation for all aspects of this project.

REFERENCES

1. Lévesque *et al.*, *NDT&E International* **39**, 622-626 (2006).
2. Stanke F. E. and Kino G. S., *J. Acoust. Soc. Am* **75**, 665-681 (1984).
3. Bolognini S. and Moreau A., *J. Appl. Phys.* **94**, 3771-3780 (2003).
4. Papadakis E.P. *et al.*, *J. Acoust. Soc. Am* **53**, 1336-1343 (1973).
5. Aussel J.-D., Monchalin J.-P., *J. Appl. Phys.* **65**, 2918-2922, (1989).
6. Weaver R.L., *Nondestructive Characterization of Materials*, **2**, Plenum Press, New York, 1987, 689–695.
7. Moreau A. *et al.*, *J. Alloy Comp.* **310**, 427-431 (2000).
8. Guo C.B. *et al*, *Acustica* **59**, 112-120 (1985).
9. Lamouche *et al.*, US Patent, 6532821 B2 (2003).
10. Prada C. *et al.*, *Wave Motion* **45**, 723-728 (2008).
11. Weaver R.L., *J. Sound and Vibration* **94**, 319-335 (1984).
12. Perton M. *et al.*, *J. Acoust. Soc. Am* ***I*26,** 1125-1130 (2009).